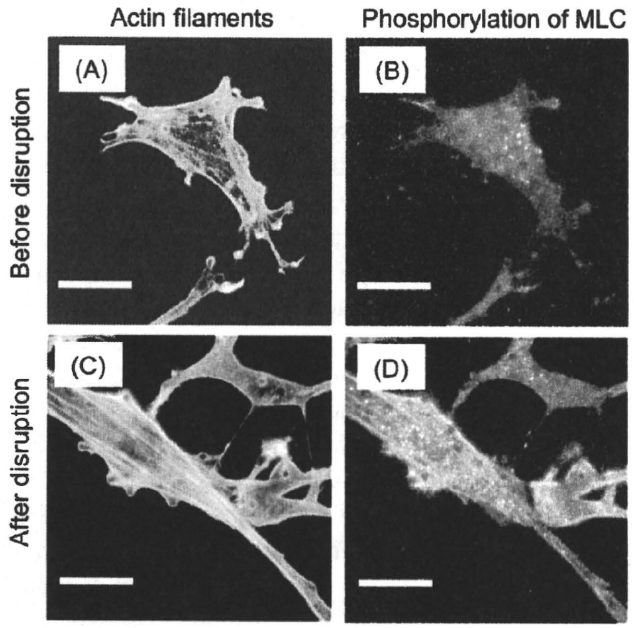

Fig. 4 Fluorescence images of actin filemant structure and phosphorylation of myosin light chain before and after disruption of microtubules. Cells stained with rhodamine-labeled phalloidin (A, C) and antibodies against phosphorylated myosin light chain (B, D). Bar = 30 μm.

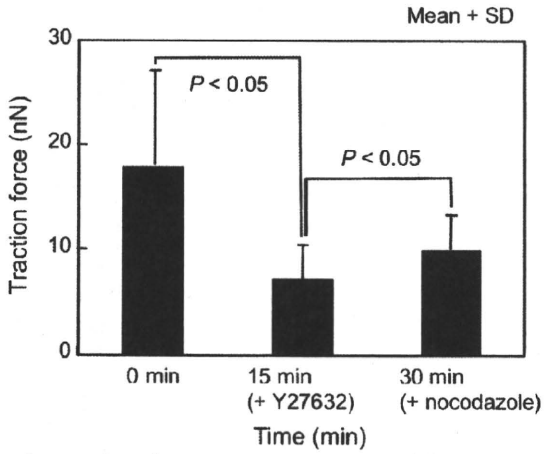

Fig. 5 Changes in traction forces after treatment with Y27632 followed by the additional treatent with nocodazole (n =5).

chain phosphorylation were then performed and showed that exposure to Y27632 significantly decreased traction forces within 15 min compared to control and the following treatment with nocodazole exhibited only 40% recovery from the prior decreased forces (Fig. 5, n = 5).

4. Discussion

Adherent cells exert traction forces to adhere to their extracellular matrix at focal adhesions and traction forces are closely related to cell physiological functions. It is thus important to know where traction forces come from and how intraellular structures such as cytoskeletons are involved in the force generation system, from the viewpoint of cell biomechanics.

As shown in Fig. 2, there was a spatial heterogeneity in traction forces. Traction forces were obviously generated towards the center of the cell, particularly indicating higher forces at the cell peripheries than at the center of the cells. Thick stress fibers seemed to be developed towards micropillars showing large deflection although the direct linkage between stress fibers and micropillars can not be observed due to probably accumulation of actin fibers around micropillars. Moreover, a close correlation of topological configuration of actin stress fibers with localozation of FAT domain was observed. These results definitely indicate that traction forces may come from intracellular tension exerted by stress fibers. The average traction forces of the cell was of the order of 10 nN. This value was consistent with that reported by Balaban et al. [3], although they used fibloblast cells and area in contact between cells and substrates is different from our study. Deguchi et al. [11] have performed tensile experiments on isolated stress fibers from smooth muscle cells and estimated that *in vivo* tension exerted on stress fibers may be of the order of 10 nN, strongly proving that stress fibers may play a major role in generation of cellular traction forces.

Tan et al. [4] have disrupted actin cytoskeleton with cytochalasin D and found that the treatment decreased traction forces, apparently indicating the mechanical contribution of actin cytoskeleton to traction forces. It should be pointed out that traction forces would be attributable to not only actin filament formation but also actin contractility. In fact, as shown in Figs. 3 and Table 1, the treatment of nocodazole disrupted microtubule structure without significant change in actin structure and incresed traction forces. Taken together, it is speculated that the increase in traction forces after the disruption of microtubules is mainly not due to change in structure of stress fibers but possibly due to an increase of contraction forces generated by stress fibers. In other words, this increase may come from activation of actomyosin contractility in stress fibers. Kolodney and Elson [7] have measured contractile forces of a population of fibroblasts populated in a collagen lattice after treatment with nocodazole and showed an increase in contractile forces. They concluded that this increase may be attributable to myosin phosphorylation leading to actomyosin force generation. In contrast, Wang et al. [12] have suggested that the shape of the cytoskeleton is stabilized predominantly by the tensile stress, which is called prestress. This tensile stress born by the actomyosin mechanism may increase cellular traction forces after disruption of microtubules that resist compression. Furthermore, they showed that microtubules contributed to > 50% of the prestress in certain cells, with the rest being balanced by the traction forces. Thus, it has still been unclear whether the increase in traction forces after disruption of microtubules may mainly not due to structural changes caused by the loss of microtubules networks but possibly due to an activation of actomyosin interactions.

It is here hypothesized that disruption of microtubules may induce phosphorylation of myosin light chain, resulting in an increaes in traction forces through activation of actomyosin contractility in stress fibers. To address this issue, we assessed whether phosphorylation of myosin light chain in stress fibers could be induced after disruption of microtubules. The result showed that myosin light chain phosphorylation was observed after the disruption of microtubles (Fig. 4). By blocking the signaling pathway, traction forces significantly decreased indicating that MLC phosphorylation could be inhibited (Fig. 5). Following treatment with nocodazole showed only 40% recovery. These results suggest that microtubules disassembly may lead to activation of actomyosin contractility in stress fibers mainly through ROCK pathway. It is also suggested that the 40% recovery is mainly due to an apparent increase in traction forces induced by the loss of

microtubules networks as compression elements. If microtubules contribute to > 50% of the prestress as suggested by Wang et al. [12], traction forces can increase by more than 100% after disruption of microtubules. However, neither in Table 1 nor in Fig. 5, the increases were not quite as high as that. This discrepancy should be carefully studied in future work. Cytoskeletal networks are an integrated system of three cytoskeletons such as actin filaments, microtubules, and intermediate filaments. These three cytoskeletons are believed to be mechanically balanced in cells, for example as suggested by Ingber [5], and should simultaneously be biochemically interrelated each other. In this regards, further study would include mechanical and biochemical contributions of intermediate filaments with implication of the other two cytoskeletons.

One of the limitations of this study is the lack of temperature control during the traction force measurements. We believe that since the measurements were performed within faster than 1 h, the effect of the change in temperature on the measurements was assumed to be negligible small. In fact, traction forces did not show a change even after 1 h under the present experimental condition. However, especially for long-term experiments such as over 1 h, experimental conditions closer to physiological conditions would be required, for instance, by introducing a microscope stage incubator to control environmental temperature.

In summary, traction forces in smooth muscle cells were here estimated by using microfabricated substrates with arrays of micropillars, particularly exploring how actin stress fibers and microtubules contribute to traction forces. The results suggest that formation and contractility of actin stress fibers are mainly involved in cellular traction forces and a contribution of microtubules is not only as a structural element involved in intracellular force balance but also rather as a modulator of the actomyosin contractile system. Such an approach utilizing the microfabricated matrix device would provide further insights to cell mechanics.

Acknowledgements

This work was supported financially in part by the Grants-in-Aid for Scientific Research (Nos. 18650119, 20001007), the 21st Century Program "Future Medical Engineering Based on Bio-nanotechnology" and Grant-in-Aid for Scientific Research on Priority Areas "System Cell Engineering by Multi-scale Manipulation", by the Ministry of Education, Culture, Sports, Science and Technology (MEXT) in Japan.

References

(1) Sheetz, M.P., Felsenfeld, D.P., Galbraith, C.G., Cell migration: regulation of force on exrtracellular-matrix-integrin complexes, *Trends in Cell Biology*, Vol. 8 (1998), pp. 51-54.

(2) Yang, J.T., Rayburn, H., Hynes, R.O., Cell adhesion events mediated by alpha 4 integrins are essential in placental and cardiac development, *Development*, Vol. 121 (1995), pp. 549-560.

(3) Balaban, N.Q., Schwarz, U.S., Riveline, D., Goichberg, P., Tzur, G., Sabanay, I., Mahalu, D., Safran, S., Bershadsky, A., Addadi, L., Geiger, B., Force and focal adhesion assembly: A close relationship studied using elastic micropatterned substrates, *Nature Cell Biology*, Vol. 3 (2001), pp. 466-472.

(4) Tan, J.L., Tien, J., Pirone, D.M., Gray, D.S., Bhadriaju, K., Chen, C.S., Cells lying on a bed of microneedles: An approach to isolate mechanical force,

Proceedings of the National Academy of Sciences, Vol. 100 (2003), pp. 1484-1489.

(5) Ingber, D.E., Tensegrity I. Cell structure and hierarchical systems biology, *Journal of Cell Science*, Vol. 116 (2003), pp. 1157-1173.

(6) Danowski, B.A., Fibroblast contractility and actin organization are stimulated by microtubule inhibitors, *Journal of Cell Science*, Vol. 93 (1989), pp. 255-266.

(7) Kolodney, M.S. and Elson, E., Contraction due to microtubule disruption is associated with increased phosphorylation of myosin regulatory light chain, *Proceedings of the National Academy of Sciences*, Vol. 92 (1995), pp. 10252-10256.

(8) Wang, N., Naruse, K., Stamenovic, D., Fredberg, J.J., Mijailovich, S.M., Tolic-Norrelykke, I.M., Polte, T., Mannix, R., Ingber, D.E., Mechanical behavior in living cells consistent with the tensegrity model, *Proceedings of the National Academy of Sciences*, Vol. 98 (2001), pp. 7765-7770.

(9) Hildebrand, J.D., Schaller, M.D., Parsons, J.T., Identification of sequences required for the efficient localization of the focal adhesion kinase, pp125FAK, to cellular focal adhesions, *Journal of Cell Biology*, Vol. 123 (1993), pp. 993-1005.

(10) Chen, C.S., Alonso, J.L., Osuni, E., Whitesides, G.M., Ingber, D.E., Cell shape provides global control of focal adhesion assembly, *Biochemical and Biophysical Research Communications*, Vol. 307 (2003), pp. 355-361.

(11) Deguchi., S., Ohashi, T., M. Sato, Tensile properties of single stress fibers isolated from cultured vascular smooth muscle cells, *Journal of Biomechanics*, Vol. 38 (2005), pp. 1751-1759.

(12) Wang, N., Tolic-Norrelykke, I.M., Chen, J., Mijailovich, S.M., Butler, J.P., Fredberg, J.J., Stamenovic, D., Cell prestress. I. Stiffness and prestress are closely associated in adherent contractile cells, *American Journal of Physiology Cell Physiology*, Vol. 282 (2002), pp. C606-C616.

Biochemical and Biophysical Research Communications 398 (2010) 426–432

Contents lists available at ScienceDirect

Biochemical and Biophysical Research Communications

journal homepage: www.elsevier.com/locate/ybbrc

Role of p120-catenin in the morphological changes of endothelial cells exposed to fluid shear stress

Naoya Sakamoto [a,*], Kei Segawa [a,1], Makoto Kanzaki [b], Toshiro Ohashi [a,2], Masaaki Sato [a,b]

[a] Department of Bioengineering and Robotics, Graduate School of Engineering, Tohoku University, Sendai, Japan
[b] Department of Biomedical Engineering, Graduate School of Biomedical Engineering, Tohoku University, Sendai, Japan

ARTICLE INFO

Article history:
Received 17 June 2010
Available online 1 July 2010

Keywords:
Endothelial cells
p120-Catenin
VE-cadherin
Fluid shear stress
Pseudopodium

ABSTRACT

p120-Catenin is known to play important roles in cell–cell adhesion stability by binding to cadherin and morphological changes of cells by regulating small RhoGTPase activities. Although the expression and binding states of p120-catenin are thought to dynamically change due to morphological adaptation of endothelial cells (ECs) to fluid shear stress, these dynamics remain to be explored. In the present study, we examined the time course of changes in p120-catenin expression and its binding to vascular endothelial (VE)-cadherin in ECs exposed to shear stress. Human umbilical vein ECs began to change their morphologies at 3–6 h, and became elongated and oriented to the direction of flow at 24 h after exposure to a shear stress of 1.5 Pa. Binding and co-localization of p120-catenin with VE-cadherin at the foci of cell–cell adhesions were retained in ECs during exposure to shear stress, indicating that VE-cadherin was stabilized in the plasma membrane. In contrast, cytoplasmic p120-catenin that was dissociated from VE-cadherin was transiently increased at 3–6 h after the flow onset. These results suggest that the transient increase of cytoplasmic p120-catenin may stimulate RhoGTPase activities and act as a switch for the morphological changes in ECs in response to shear stress.

1. Introduction

Vascular endothelial cells (ECs) are generally known to exhibit structural and functional adaptations to fluid shear stress arising from blood flow [1,2]. ECs become elongated and aligned with the direction of flow concomitant with the reorganization of their cytoskeletal structure, including actin filaments, after exposure to fluid shear stress [3,4]. In addition, many EC functions such as the regulation of barrier permeability between blood and underlying tissues are also affected by shear stress [5]. Because ECs are believed to significantly contribute to pathophysiological changes of vessel walls, the mechanisms associated with EC flow adaptation have been investigated.

ECs line blood vessels as monolayers by the formation of intercellular adherens junctions that are mediated by vascular endothelial cadherin (VE-cadherin), which is one of the cell–cell adhesion molecules that are selectively expressed by ECs. VE-cadherin mediates intercellular adherens junction formation via Ca^{2+}-dependent homophilic interactions of its ectodomain and association of its cytoplasmic domain to catenins, such as α- and β-catenins, which contribute to the anchorage between VE-cadherin and the actin cytoskeleton. The adherens junction is associated with vascular permeability and, as a consequence, the pathogenesis of atherosclerotic vascular diseases. It has been reported that a mutant VE-cadherin lacking an adhesive extracellular domain disrupted EC endothelial barrier function [6]. In addition to the barrier function, the adherens junction has recently been implicated in the activation of critical intracellular signaling molecules, such as Akt kinases and NF-κB (nuclear factor of kappa light chain gene enhancer in B cells), associated with EC morphological and functional responses to shear stress [7–9]. Inhibition of adherens junction constitution resulted in reduced production of a vasoconstrictor peptide, endothelin [10], and ECs that did not form intercellular adhesions did not morphologically respond to shear stimulation [3,11]. Therefore, the integrity of cell–cell adhesions via VE-cadherin is required for EC physiological functions and morphological changes during EC adaptations to shear stress.

The functions of VE-cadherin are regulated by its interactions with catenins. p120-Catenin, a catenin that binds to VE-cadherin and does not interact with the actin cytoskeleton, has recently come into focus because of its important role in the integrity of adherens junction and morphological changes in ECs. Previous studies showed that depletion of p120-catenin by small interfering

* Corresponding author. Address: Department of Bioengineering and Robotics, Graduate School of Engineering, Tohoku University, Aramaki Aza, Aoba, 6-6-01 Sendai 980-8579, Japan. Fax: +81 22 795 6945.
E-mail address: naoya@bml.mech.tohoku.ac.jp (N. Sakamoto).
[1] Present address: Teijin Pharma Ltd., Japan.
[2] Present address: Division of Human Mechanical Systems and Design, Faculty of Engineering, Hokkaido University, Sapporo, Hokkaido, Japan.

0006-291X/$ - see front matter © 2010 Elsevier Inc. All rights reserved.
doi:10.1016/j.bbrc.2010.06.092

RNA resulted in a loss of cadherin expression and adherens junction [12,13]. Binding of p120-catenin prevented clathrin-dependent endocytosis of VE-cadherin, indicating that p120-catenin stabilized VE-cadherin in the plasma membrane [14]. In addition, cytoplasmic p120-catenin that is dissociated from VE-cadherin acts as a regulator of the activities of RhoGTPases, such as RhoA, Rac1, and Cdc42, which are involved in cell migration and morphological changes via the formation of pseudopods and actin stress fibers [15]. These findings suggest a hypothesis that p120-catenin binding to VE-cadherin contributes to the stabilization of cell–cell adhesions, while p120-catenin that is dissociated from VE-cadherin contributes to actin reorganization during EC remodeling in response to fluid shear stress.

However, few studies have investigated the effects of shear stress on p120-catenin, and the role of p120-catenin in morphological responses of ECs to shear stress is poorly understood. To test this hypothesis, we investigated the expression and association of p120-catenin with VE-cadherin during the process of morphological changes induced in ECs by shear stress.

2. Materials and methods

2.1. Cell culture

ECs were harvested from veins of human umbilical cords using an enzyme digestion method [16]. The cells were cultured in Medium199 (Invitrogen, USA) supplemented with 20% heat-inactivated fetal bovine serum (JRH Bioscience, USA), 10 U/ml penicillin, 10 μg/ml streptomycin, and 10 ng/ml human basic fibroblast growth factor (bFGF, Austral Biologicals, USA) at 37 °C in a humidified incubator (Thermo Scientific, USA) with 5% CO_2. For experiments, ECs subcultured at passages 3–6 were plated onto glass-based dishes (ϕ35, Asahi Techno Glass, Japan) or cell culture dishes (ϕ90, Sumiron, Japan) coated with 0.1% gelatin.

2.2. Flow exposure experiment

Steady laminar flow was applied at shear stress of 1.5 Pa to confluent ECs using a parallel plate flow chamber system [4]. A peristaltic pump (Masterflex, USA) was used to propel the culture medium from a reservoir through the flow chamber. A second sealed reservoir was placed between the pump and flow chamber to eliminate pulsations. The culture medium was maintained at 37 °C and equilibrated with 5% CO_2 throughout the experiment.

2.3. Fluorescent staining

ECs were fixed with 2% paraformaldehyde in physiological buffered saline (PBS) containing 0.5 mM $MgCl_2$ and 1 mM $CaCl_2$ for 5 min, washed 2 times with PBS, permeabilized with 0.2% Triton X-100 for 10 min, and blocked with 25% Block Ace (Dainippon Pharma, Japan) in PBS for 30 min at room temperature. Cells were incubated overnight at 4 °C with mouse monoclonal antibodies directed against VE-cadherin (Santa Cruz Biotechnology, USA) and p120-catenin (BD Biosciences, USA). Cells were then washed twice with PBS and incubated with anti-mouse Alexa Fluor 488-conjugated antibodies for 1 h at room temperature. Subsequently, EC actin filaments were stained with 2.5 U/ml rhodamine–phalloidin (Invitrogen, USA) for 20 min. Fluorescent images of cells were obtained by confocal laser scanning microscopy (Olympus, Japan).

2.4. Morphological analysis

Fluorescent images were analyzed to determine EC morphological parameters using ImageJ software (National Institutes of Health, USA). EC morphology was evaluated on the basis of two parameters: aspect ratio and angle of cell orientation. The aspect ratio was defined as the ratio between the minor and major axes of an ellipse equivalent to the cell shape. The aspect ratio has a maximum value of 1 for a perfect circle and approaches 0 for highly elongated shapes. The angle of cell orientation was defined as the angle of the long axis of the equivalent ellipse with respect to the direction of flow. The distributions of the orientation angle are given as circular histograms to illustrate the orientations of cells relative to the direction of flow.

2.5. Extraction of cell proteins

After the flow exposure experiments, ECs were incubated with 100 μM Na_3NO_4 in Medium199 containing 10 ng/ml human bFGF for 7 min at 37 °C prior to protein extraction. Cells were washed with ice-cold PBS and lysed in ice-cold Triton/NP-40 lysis buffer (50 mM Tris–Cl, 150 mM NaCl, 1 mM EDTA, 1% Triton X-100, 1% NP-40, 6.5 IU/μl aprotinin, 100 μM phenilmethylsulfonyl fluoride (PMSF), 5 μg/ml leupeptin, 1 μg/ml pepstatin A, 300 μM Na_3VO_4, 10 mM NaF, pH 7.5) for 5 min. The lysates were centrifuged and the supernatants were recovered.

2.6. Western blotting

The extracted protein samples were solubilized in sample buffer, separated by SDS–PAGE (8% polyacrylamide), and transferred to a PVDF membrane. The membrane was blocked with 5% bovine serum albumin blocking buffer (20 mM Tris–hydroxymethilaminomethane, 137 mM NaCl, 0.1% Tween 20, 0.02% NaN_3) for 30 min at room temperature, incubated with mouse monoclonal antibodies against VE-cadherin or p120-catenin overnight at 4 °C, and then probed with horseradish peroxidase-conjugated anti-mouse antibodies for 1 h. Signals were detected using SuperSignal West Pico chemiluminescent substrate (Pierce, USA).

2.7. Immunoprecipitation

The extracted protein samples were incubated on a rotator overnight at 4 °C with mouse monoclonal antibodies against VE-cadherin and then for 2 h with protein G-Sepharose. The immunoprecipitated samples were collected by centrifugation and washed 3 times with IP buffer (50 mM Tris–Cl, 150 mM NaCl, 1 mM EDTA, 1% Triton X-100, 6.5 IU/μl aprotinin, 100 μM PMSF, 5 μg/ml leupeptin, 1 μg/ml pepstatin A, 300 μM Na_3VO_4, 10 mM NaF, pH 7.5). The washed pellets were resuspended in sample buffer and boiled for 7 min. The supernatants were analyzed as described above for Western blotting.

3. Results

3.1. Morphological changes in ECs after exposure to shear stress

The time course of EC cytoskeletal and morphological changes induced by shear stress were examined by immunofluorescent microscopy and image analysis (Figs. 1 and 2). Under static conditions, ECs exhibited characteristic cobblestone shapes and VE-cadherin was continuously expressed at cell–cell junctions, as reported previously [17] (Fig. 1A–C). After exposure to shear stress for 3 and 6 h, the dense peripheral bands of actin filaments that were observed under static conditions became less prominent (Fig. 1D–I). VE-cadherins accumulated in a striped pattern and were co-localized with actin filament terminals in regions of the cell periphery, indicating that the cells had developed interconnected pseudopod-

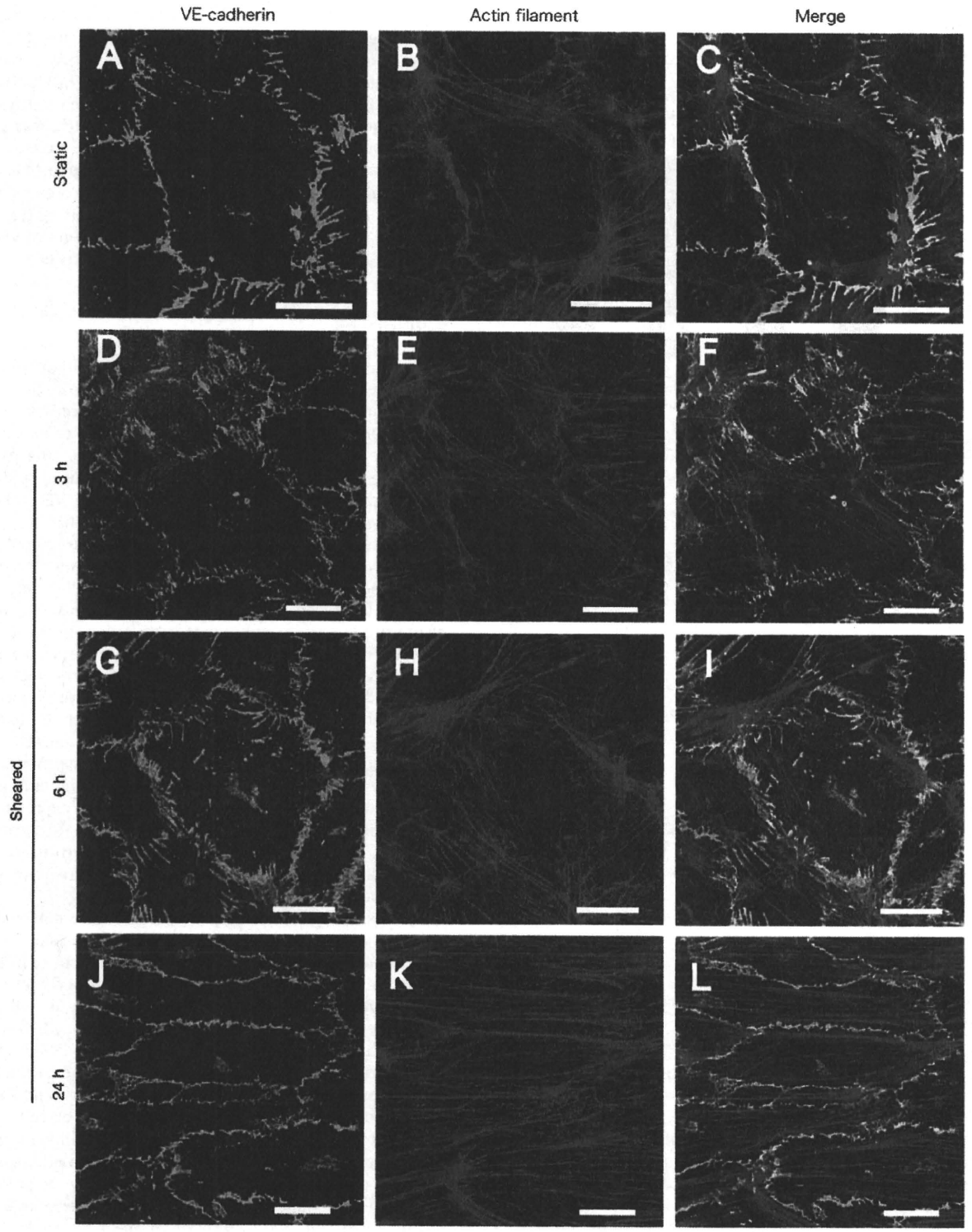

Fig. 1. Representative fluorescent images of VE-cadherin and actin filaments of ECs cultured statically (A–C) and exposed to a shear stress of 2 Pa for 3 h (D–F), 6 h (G–I), and 24 h (J–L). (A, D, G, J) VE-cadherin. (B, E, H, K) Actin filaments. (D, F, I, L) Merged images. The direction of flow is left to right. Bar = 20 μm.

like processes [18]. At 24 h, almost all the cells were elongated and orientated to the direction of flow. VE-cadherins were again continuously distributed around cell peripheries (Fig. 1J–L).

Fig. 2A shows the EC aspect ratios. Up to 6 h after exposure to shear stress, the EC aspect ratios were approximately 0.6, which were comparable to those under static conditions. The aspect ratio then showed a significant decrease after 24 h of shear stress. Changes in the distribution of orientation angles are indicated in Fig. 2B. ECs were randomly oriented prior to exposure to shear stress, and then began to orient in the direction of flow at 3 h after flow onset. More than 50% of ECs were aligned with their orientation angles in the range of ±30° to the direction of flow after exposure to shear stress for 6 h, and 85% cells were orientated in the range of ±30° to the direction of flow at 24 h.

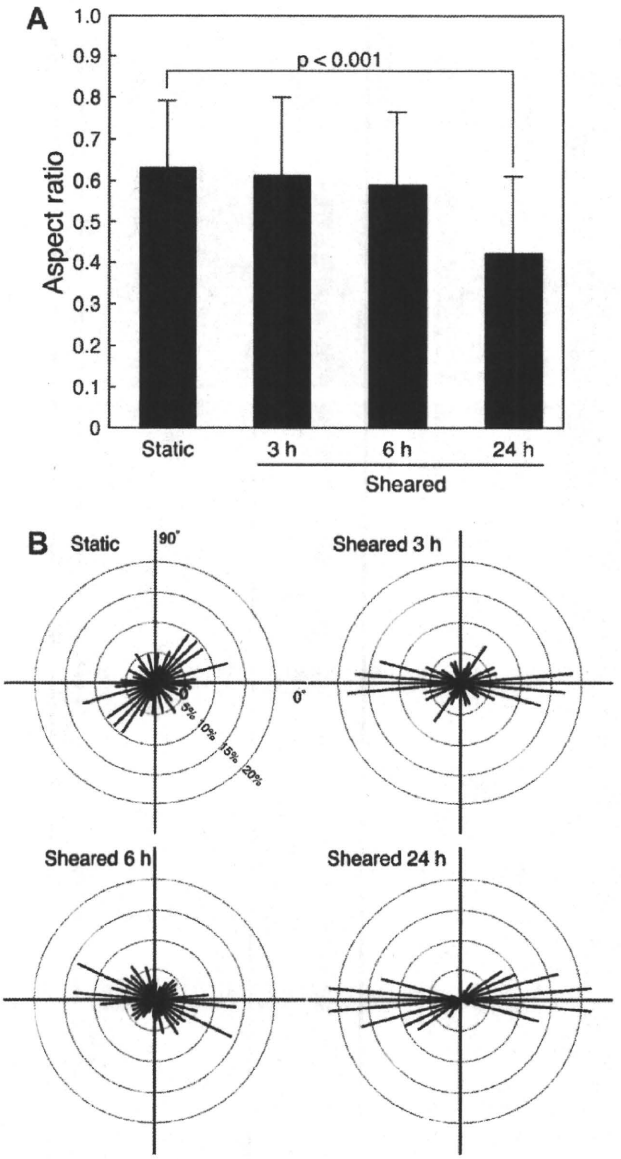

Fig. 2. Morphological analyses of ECs. (A) Aspect ratios of ECs. Results are expressed as mean + SD. (B) Angles of cell orientation. Lengths and bar angles indicate relative frequencies and cell orientation angles, respectively.

3.2. Changes in p120-catenin distribution after exposure to shear stress

Fig. 3 shows images of double-immunofluorescent staining for VE-cadherin and p120-catenin of ECs exposed to shear stress. The continuous localization of p120-catenin was observed at cell–cell junctions and was co-localized with VE-cadherin under static conditions. After exposure to shear stress for up to 24 h, p120-catenin was continuously expressed at intercellular junctions and maintained its co-localization with VE-cadherin.

3.3. Changes in VE-cadherin and p120-catenin expressions after exposure to shear stress

Western blotting of whole-cell lysates revealed that VE-cadherin expression by ECs exposed to shear stress did not change compared to that under static conditions (Fig. 4A). Western blotting performed for p120-catenin detected 2 bands at 100 and 115 kDa (Fig. 4B). It has been reported that many types of cells express multiple isoforms of p120-catenin that are derived by alternative splicing of a single gene [19], and each isoform has a domain that interacts with cadherins. In the present study, the levels of both the higher (115 kDa) and lower (100 kDa) molecular weight p120-catenin in whole-cell lysates transiently increased at 3 and 6 h after exposure to shear stress. The expression of p120-catenin then returned to the basal level at 24 h. In contrast, for ECs exposed to shear stress for up to 24 h, no significant change was observed in the level of p120-catenin detected by immunoprecipitation followed by Western blotting (Fig. 4C). This indicated that the amount of p120-catenin bound to VE-cadherin in ECs was unchanged after exposure to shear stress.

4. Discussion

Immunofluorescent microscopy revealed that p120-catenin maintained its co-localization with VE-cadherin at the peripheries of ECs during the morphological changes induced by shear stress. In addition, the amount of p120-catenin bound to VE-cadherin detected by immunoprecipitation did not change after exposure to shear stress. The EC morphological changes induced by shear stress are thought to involve, in part, the dissociation of VE-cadherin binding between neighboring cells. VE-cadherins that are dissociated from junctions are known to be incorporated into a cytoplasmic pool by endocytosis or are maintained in the plasma membrane, called a plasma membrane pool. Because binding of p120-catenin has been reported to prevent endocytosis of VE-cadherins [14], the results of the present study indicate that VE-cadherin dissociated from adherens junctions is continuously present in the plasma membrane when ECs undergo morphological changes. Ukropec et al. [20] reported a decreased amount of α-catenin that was associated with VE-cadherin in ECs after exposure to shear stress for 3–6 h, which suggested a loss of linkage between VE-cadherin and actin filaments. After dissociating from actin filaments, VE-cadherin–p120-catenin complexes may freely move within the plasma membrane. In the present study, a striped pattern of VE-cadherin expression at cell–cell junctions was observed after exposing cells to shear stress for 3 and 6 h. This phenomenon may have been due to an accumulation of VE-cadherin–p120-catenin complexes that freely moved in the membrane.

Increased expressions of p120-catenin were detected by Western blotting of whole-cell lysates from ECs that had been exposed to shear stress for 3 and 6 h. Because the amount of p120-catenin bound to VE-cadherin detected by immunoprecipitation did not change after exposure to shear stress, this result indicated that shear stress induced an increased amount of cytoplasmic p120-catenin that was not bound to VE-cadherin in ECs from 3 to 6 h. Several studies have indicated that cytoplasmic p120-catenin induces activation of RhoGTPases, including Cdc42 and Rac1, which are regulators of actin cytoskeletal networks at cell peripheries and lead to the formation of filopodia and lamellipodia. In addition to cell migration, these pseudopod formations are thought to be involved in the morphological changes of cells. In the present study, formation of pseudopod-like processes at cell peripheries were observed when cells were exposed to shear stress for 3 and 6 h (Fig. 1D–I), which was followed by significant cell elongation and their alignment in the direction of flow (Fig. 2). Thus, these morphological changes could be triggered by the increased cytoplasmic p120-catenin under shear conditions. At 24 h, p120-catenin expression decreased and returned to a level comparable to that under static conditions. This may indicate that the activities of Rac1 and Cdc42 had decreased and that changes in EC morphology in response to shear stress may have been completed.

Although a part of the observed expression of VE-cadherin was punctuated, adherens junctions comprising VE-cadherin were

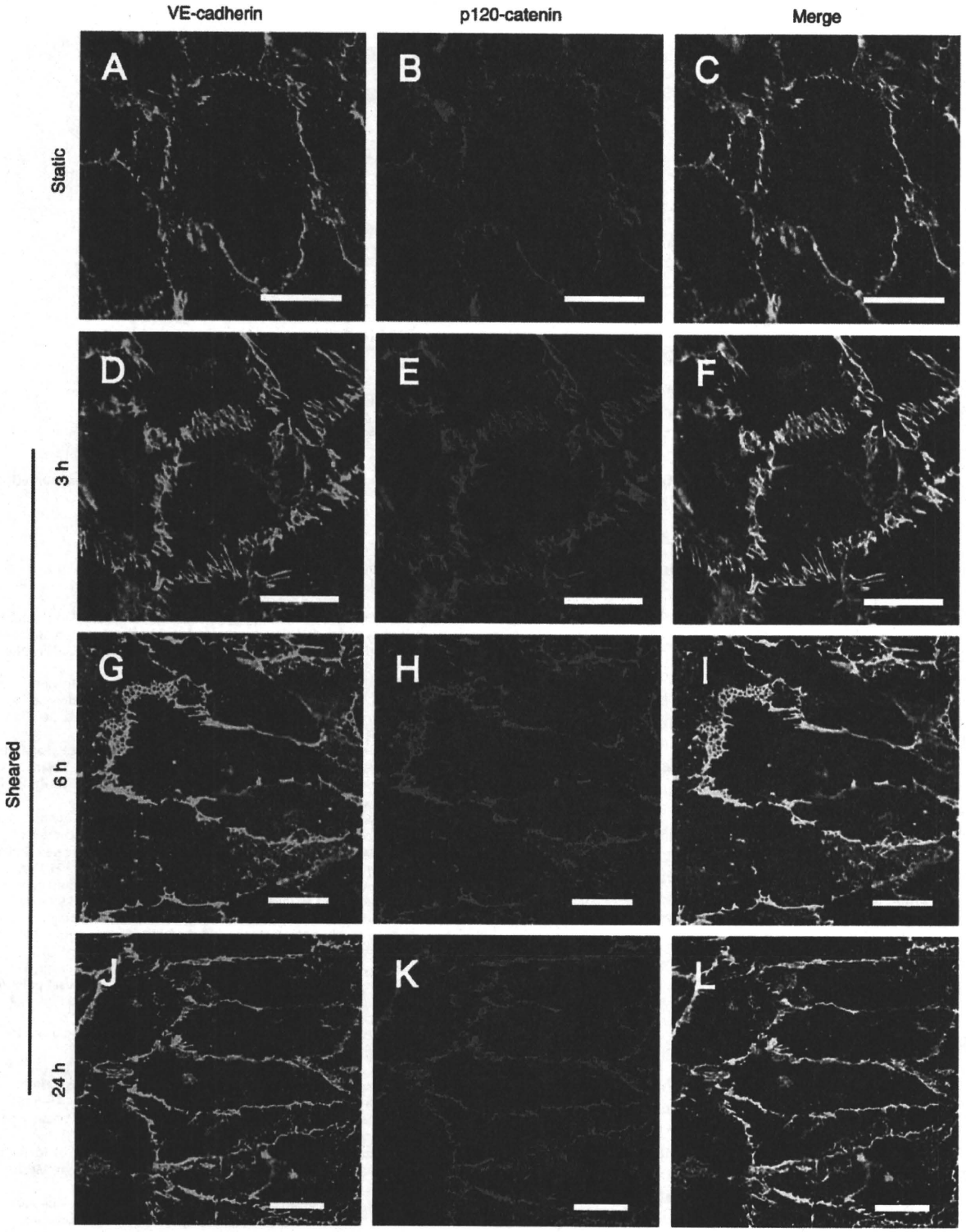

Fig. 3. Representative fluorescent images of VE-cadherin and p120-catenin of ECs cultured statically (A–C) and exposed to a shear stress of 2 Pa for 3 h (D–F), 6 h (G–I), and 24 h (J–L). (A, D, G, J) VE-cadherin. (B, E, H, K) p120-catenin. (D, F, I, L) Merged images. The direction of flow is left to right. Bar = 20 μm.

primarily formed at EC intercellular junctions during morphological changes in response to shear stress. This is consistent with the results of a previous report [17] and indicates that ECs that morphologically adapt to shear stress strictly maintain their intercellular adhesion integrity. The integrity of adherens junctions via VE-cadherin influences permeability of the endothelium, and abnormally higher permeability is often observed at inflammatory sites and regions that are prone to the development of atherosclerotic plaques [21]. The initiation of the formation of intercellular adhesions via cadherin is thought to be a result of the redistribution and punctuation of surface-bound cadherin, rather than the recruitment of cadherin from cytoplasmic pools, and is followed

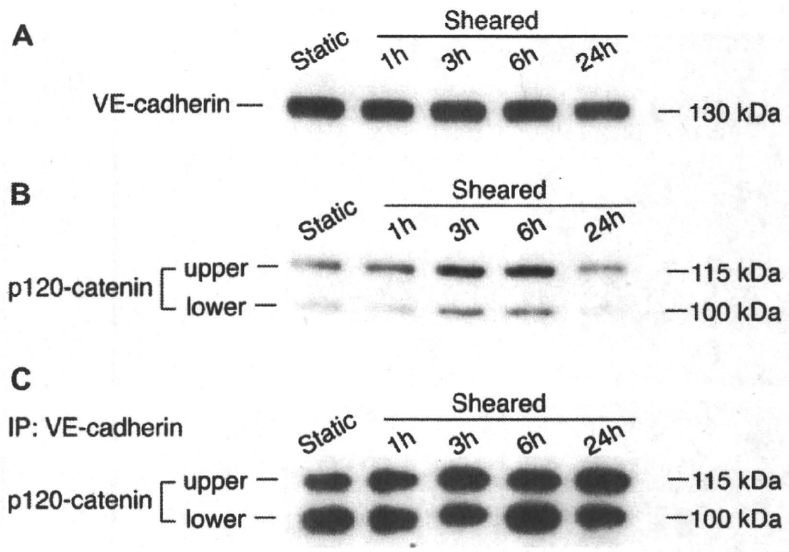

Fig. 4. Representative results of Western blotting. (A) VE-cadherin and (B) p120-catenin detected in whole-cell lysates and (C) p120-catenin immunoprecipitated from whole-cell lysates. The results shown are representative of three independent experiments.

by stabilization with the assembly of additional cadherin and connections with the cytoskeleton [22–24]. Further, because cadherin that lacks a cytoplasmic tail for binding to p120-catenin cannot form clusters, p120-catenin is required for VE-cadherin clustering and stabilizing cell–cell adhesions [25,26]. Taken together, p120-catenin may maintain the presence of VE-cadherin on the plasma membrane, which plays an important role in rapid cluster formation of VE-cadherin at intercellular junctions during flow-induced morphological changes. This could lead to reducing the increased endothelial permeability due to the dissociation of VE-cadherin.

In summary, the present study showed that p120-catenin in ECs maintained its binding and co-localization with VE-cadherin and contributed to stabilizing adherens junctions during morphological responses to shear stress. In addition, the expression of cytoplasmic p120-catenin increased at 3 and 6 h after exposure to shear stress. Because cytoplasmic p120-catenin is known to regulate the activities of RhoGTPases (including CdC42 and Rac1), which leads to the formation of filopodia and lamellipodia, the increased cytoplasmic p120-catenin may act as a switch that induces EC morphological changes in response to flow.

Acknowledgments

The authors would like to thank Drs. Makoto Takahashi and Ikuo Takahashi for kindly providing human umbilical cords with the informed consent of donors. This study was supported in part by Grants-in-Aid for Scientific Research from the Ministry of Education, Culture, Sports, Science and Technology (MEXT) of Japan (Nos. 20001007 and 21700457), and the Mitsubishi Foundation.

References

[1] A.M. Malek, S.L. Alper, S. Izumo, Hemodynamic shear stress and its role in atherosclerosis, JAMA 282 (1999) 2035–2042.
[2] B.P. Helmke, Molecular control of cytoskeletal mechanics by hemodynamic forces, Physiology (Bethesda) 20 (2005) 43–53.
[3] N. Kataoka, S. Ujita, M. Sato, Effect of flow direction on the morphological responses of cultured bovine aortic endothelial cells, Med. Biol. Eng. Comput. 36 (1998) 122–128.
[4] N. Sakamoto, T. Ohashi, M. Sato, Effect of fluid shear stress on migration of vascular smooth muscle cells in cocultured model, Ann. Biomed. Eng. 34 (2006) 408–415.
[5] O. Ogunrinade, G.T. Kameya, G.A. Truskey, Effect of fluid shear stress on the permeability of the arterial endothelium, Ann. Biomed. Eng. 30 (2002) 430–446.
[6] K. Venkiteswaran, K. Xiao, S. Summers, C.C. Calkins, P.A. Vincent, K. Pumiglia, A.P. Kowalczyk, Regulation of endothelial barrier function and growth by VE-cadherin, plakoglobin, and beta-catenin, Am. J. Physiol. Cell Physiol. 283 (2002) C811–C821.
[7] A. Shay-Salit, M. Shushy, E. Wolfovitz, H. Yahav, F. Breviario, E. Dejana, N. Resnick, VEGF receptor 2 and the adherens junction as a mechanical transducer in vascular endothelial cells, Proc. Natl. Acad. Sci. USA A99 (2002) 9462–9467.
[8] P. Turowski, R. Martinelli, R. Crawford, D. Wateridge, A.P. Papageorgiou, M.G. Lampugnani, A.C. Gamp, D. Vestweber, P. Adamson, E. Dejana, J. Greenwood, Phosphorylation of vascular endothelial cadherin controls lymphocyte emigration, J. Cell Sci. 121 (2008) 29–37.
[9] E. Tzima, M. Irani-Tehrani, W.B. Kiosses, E. Dejana, D.A. Schultz, B. Engelhardt, G. Cao, H. DeLisser, M.A. Schwartz, A mechanosensory complex that mediates the endothelial cell response to fluid shear stress, Nature 437 (2005) 426–431.
[10] F. Kiessling, D. Becker, E.V. Ullisch, W. Kubler, C. Haller, Influence of intercellular junctions on endothelin secretion of human umbilical vein endothelial cells in vitro, Basic Res. Cardiol. 95 (2000) 299–307.
[11] M. Masuda, K. Fujiwara, Morphological responses of single endothelial cells exposed to physiological levels of fluid shear stress, Front. Med. Biol. Eng. 5 (1993) 79–87.
[12] K. Xiao, D.F. Allison, K.M. Buckley, M.D. Kottke, P.A. Vincent, V. Faundez, A.P. Kowalczyk, Cellular levels of p120 catenin function as a set point for cadherin expression levels in microvascular endothelial cells, J. Cell Biol. 163 (2003) 535–545.
[13] M.A. Davis, R.C. Ireton, A.B. Reynolds, A core function for p120-catenin in cadherin turnover, J. Cell Biol. 163 (2003) 525–534.
[14] K. Xiao, J. Garner, K.M. Buckley, P.A. Vincent, C.M. Chiasson, E. Dejana, V. Faundez, A.P. Kowalczyk, p120-catenin regulates clathrin-dependent endocytosis of VE-cadherin, Mol. Biol. Cell 16 (2005) 5141–5151.
[15] P.Z. Anastasiadis, A.B. Reynolds, Regulation of Rho GTPases by p120-catenin, Curr. Opin. Cell Biol. 13 (2001) 604–610.
[16] N. Sakamoto, T. Ohashi, M. Sato, Effect of magnetic field on nitric oxide synthesis of cultured endothelial cells, Int. J. Electromagn. Mech. (2000) 317–322.
[17] S. Noria, D.B. Cowan, A.I. Gotlieb, B.L. Langille, Transient and steady-state effects of shear stress on endothelial cell adherens junctions, Circ. Res. 85 (1999) 504–514.
[18] S. Kostin, S. Hein, E.P. Bauer, J. Schaper, Spatiotemporal development and distribution of intercellular junctions in adult rat cardiomyocytes in culture, Circ. Res. 85 (1999) 154–167.
[19] J.M. Staddon, C. Smales, C. Schulze, F.S. Esch, L.L. Rubin, p120, a p120-related protein (p100), and the cadherin/catenin complex, J. Cell Biol. 130 (1995) 369–381.
[20] J.A. Ukropec, M.K. Hollinger, M.J. Woolkalis, Regulation of VE-cadherin linkage to the cytoskeleton in endothelial cells exposed to fluid shear stress, Exp. Cell Res. 273 (2002) 240–247.
[21] R.A. Herrmann, R.A. Malinauskas, G.A. Truskey, Characterization of sites with elevated LDL permeability at intercostal, celiac, and iliac branches of the normal rabbit aorta, Arterioscler. Thromb. 14 (1994) 313–323.

[22] C.L. Adams, Y.T. Chen, S.J. Smith, W.J. Nelson, Mechanisms of epithelial cell–cell adhesion and cell compaction revealed by high-resolution tracking of E-cadherin-green fluorescent protein, J. Cell Biol. 142 (1998) 1105–1119.
[23] A. Kusumi, K. Suzuki, K. Koyasako, Mobility and cytoskeletal interactions of cell adhesion receptors, Curr. Opin. Cell Biol. 11 (1999) 582–590.
[24] K. Noda, J. Zhang, S. Fukuhara, S. Kunimoto, M. Yoshimura, N. Mochizuki, Vascular endothelial-cadherin stabilizes at cell–cell junctions by anchoring to circumferential actin bundles through alpha- and beta-catenins in cyclic AMP-Epac-Rap1 signal-activated endothelial cells, Mol. Biol. Cell 21 (2010) 584–596.
[25] A.S. Yap, C.M. Niessen, B.M. Gumbiner, The juxtamembrane region of the cadherin cytoplasmic tail supports lateral clustering, adhesive strengthening, and interaction with p120ctn, J. Cell Biol. 141 (1998) 779–789.
[26] P.Z. Anastasiadis, A.B. Reynolds, The p120 catenin family: complex roles in adhesion, signaling and cancer, J. Cell Sci. 113 (Pt. 8) (2000) 1319–1334.

Size sorting of kinesin-driven microtubules with topographical grooves on a chip†

Shukei Sugita,‡*[a] Tatsuya Murase,[b] Naoya Sakamoto,[b] Toshiro Ohashi§[b] and Masaaki Sato[ab]

Received 28th September 2009, Accepted 4th December 2009
First published as an Advance Article on the web 6th January 2010
DOI: 10.1039/b920164e

Gliding microtubules (MTs) on a surface coated with kinesin biomolecular motors have been suggested for the development of nanoscale transport systems. In order to establish a sorting function for gliding MTs, events for MTs approaching micro-scale grooves were investigated. MTs longer than the width of grooves fabricated on a Si substrate bridged the grooves (bridging) and many MTs shorter than the groove width almost began to bridge, but returned to the surface that they approached from (guiding). Occurrence probabilities for the events were analyzed with focus on the geometric conditions, such as length of the MTs, width of the grooves, and the incident angle (α) of the MTs approaching the grooves. The occurrence probability for bridging increased with an increase in the incident angle (16%, α = 0–30°; 51%, α = 30–60°; 75%, α = 60–90°), and the probability for guiding decreased with an increase in the incident angle (79%, α = 0–30°; 55%, α = 30–60°; 5%, α = 60–90°). The results indicate that an incident angle of 30–60° is an effective condition for MT sorting, because the bridging and guiding events can sort MTs that are longer and shorter than the groove widths, respectively. Furthermore, the occurrence probabilities of both bridging and guiding in a higher concentration of methylcellulose (0.5%) increased up to approximately 70% at incident angles of 30–60°, indicating good feasibility for the development of devices for the sorting of MTs on surfaces with topographical grooves.

1. Introduction

Kinesin motor proteins move along the cytoskeletal networks of microtubules (MTs) to transport protein-containing vesicles in cells. Recently, several studies suggested that *in vitro* MT–kinesin interactions could potentially be used as a bio-actuator for nanoscale transport systems.[1,2] In such systems, MTs gliding on a kinesin-coated surface have been suggested as transporters that carry nanoscale cargos to destinations. To date, there have been many studies that have reported establishing functions, such as the loading of cargo onto the MTs,[3] unidirectional transport of MTs with topological guides,[3,4] and control of the gliding direction of MTs with application of external forces.[5–7] In addition to these, the sorting of transporters is a required function for the transport of cargo to desired destinations in a system. van den Heuvel *et al.*[8] showed that rhodamine- and fluorescein isothiocyanate (FITC)-conjugated MTs were sorted into two different reservoirs by application of an electric field perpendicular to the gliding directions of the MTs at the Y-junction of a channel. Although high sorting efficiency of approximately 70% was reported for the device, additional devices were required for application of the electric field and functions such as recognition of colors of the MTs. To develop simple and compact transport systems, it is more desirable to fabricate a device that automatically sorts the MTs without the need for additional devices and functions.

Hess *et al.*[1] observed that MTs shorter than the width of a groove, which was topographically fabricated with a photoresist layer on a substrate, fell into the groove (falling), whereas MTs longer than the groove width bridged the groove and continued movement on the opposite side (bridging). We suggest that the relationship between the MT length and the groove width is applicable to the development of a sorting in which MTs are sorted by the difference in their lengths, without the need for additional devices.

In this paper, details of the behavior of kinesin-driven MTs approaching micro-scale grooves fabricated on a chip were analyzed with focus on the relationship between the lengths of the MTs and widths of the grooves. As a result, five events were observed over grooves and their probabilities were analyzed for the establishment of an MT sorting function. Furthermore, effective conditions for sorting, including geometric and solution conditions were investigated.

2. Experimental

Fabrication of microgrooves

A Si wafer (thickness = 200 μm, 2 × 2 cm², KN Platz, Osaka, Japan) was cleaned by ultrasonication in a surface-active agent

[a]*Department of Biomedical Engineering, Graduate School of Biomedical Engineering, Tohoku University, 6-6-01 Aramaki-aza-Aoba, Aoba, Sendai, 980-8579, Japan*
[b]*Department of Bioengineering and Robotics, Graduate School of Engineering, Tohoku University, 6-6-01 Aramaki-aza-Aoba, Aoba, Sendai, 980-8579, Japan*

† Electronic supplementary information (ESI) available: Movies and measurements of adhesion and motility properties of microtubules on gold-coated surfaces compared with glass and silicon surfaces. See DOI: 10.1039/b920164e

‡ Present address: Nagoya Institute of Technology, Center for Fostering Young and Innovative Researchers, Gokiso-cho, Showa-ku, Nagoya 466-8555, Japan. E-mail: sugita.shukei@nitech.ac.jp. Fax: +81 52 735 5678; Tel: +81 52 735 5678

§ Present address: Division of Human Mechanical Systems and Design, Graduate School of Engineering, Hokkaido University, N13, W8, Kita, Sapporo 060-8628, Japan.

for 10 min and then in methanol for 15 s. After submersion in Piranha solution (a strongly oxidizing mixture of hydrogen peroxide (H_2O_2, 30%) and sulfuric acid (H_2SO_4, 97%) in a volume ratio of 1 : 2) for 15 min, the wafer was immersed in a 1 : 1 : 6 mixture solution of H_2SO_4, H_2O_2, and ammonium hydroxide (NH_4OH, 29%) for 15 min to remove dust. The wafer was then rinsed four times in deionized distilled water (ddH_2O) and spin-dried. The wafer was then heat treated on a hot plate at 180 °C for 3 min.

Schematic illustrations of the micro-groove fabrication process are shown in Fig. 1A. A 450 nm thick layer of electron-beam-sensitive resist (ZEP520A; methyl styrene chloromethyl acrylate copolymer in methoxybenzene, Zeon Corporation, Tokyo, Japan) was spin-coated (5000 rpm for 3 s followed by 4000 rpm for 60 s) onto the substrate, followed by heat treatment on a hot plate at 180 °C for 3 min. Four different widths (2, 4, 6, and 10 μm) of line patterns were designed with computer aided design (CAD) software and were generated on the resist with an electron-beam lithography system (ELS-3700, Elionix, Tokyo, Japan) using a dose of 35 mJ/cm^2. The wafer was developed by immersion in a developer of n-amyl acetate (ZED-N50, Zeon Corporation) for 2 min and then immersed in methyl isobutyl ketone (MIBK, Wako, Osaka, Japan) for 1 min to stop the development, followed by rinsing in ddH_2O. The wafer was then dried with nitrogen and heat treated on a hot plate at 110 °C for 3 min.

A deep reactive-ion etching (RIE) Bosch process was used to create deep grooves with steep sidewalls. The wafer was etched for 30 min in sulfur hexafluoride (SF_6) for plasma etching and octafluorocyclobutane (C_4F_8) to form a chemically inert passivation layer. The wafer was then immersed in a positive-resist stripper of N-methyl-2-pyrrolidone (MS2001, Fujifilm, Tokyo, Japan) for 15–20 min to remove the resist. The wafer was washed in Piranha solution for 15 min, and rinsed four times in ddH_2O. After the wafer was spin-dried, a 20 nm adhesion layer of Cr and a 20 nm thick layer of Au were sequentially deposited on the Si wafer using sputtering apparatus (CFS-4ES, Shibaura, Ebina, Japan).

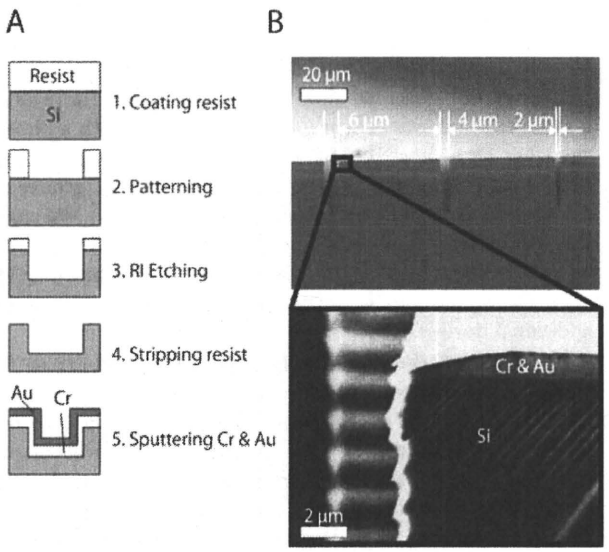

Fig. 1 Microscale grooves fabricated on an Au-coated Si substrate. (A) Cross-sectional schematic illustrations of the groove fabrication process. After line patterns were prepared, reactive ion etching (RIE) was used to fabricate the grooves with steep sidewalls. Layers of Cr followed by Au were then deposited to improve the motility properties of gliding MTs on the substrate. (B) Scanning electron microscope images of the grooves. One of the edges of a groove in the low-resolution image (top) is enlarged in the bottom image.

Motility assays

Preparation of kinesin motor proteins and rhodamine-labeled MTs, and the motility assays were performed according to a previous report.[9] All solutions were prepared using a slightly modified BRB80 buffer (80 mM PIPES, 1 mM EGTA, 4 mM $MgSO_4$, pH 6.9). Bovine tubulins containing 20% rhodamine-labeled tubulins were incubated in the BRB80 buffer including 1 mM guanosine 5′-triphosphate (GTP) at 37 °C for 1 h to polymerize MTs. *Drosophila* kinesins[10] with biotin carboxyl carrier protein at the C-terminal[11] were used. A flow cell was fabricated for observation of the gliding MTs on the kinesin-coated surface by sandwiching 22 μm thick spacers with a coverslip (24 × 36 mm^2, No.1, Matsunami, Osaka, Japan) and the prepared substrates with micro-grooves. The flow cell was sequentially filled with 1 mg/mL of biotinylated bovine serum albumin (BSA), 1 mg/mL of streptavidin, 38 μg/mL of biotinylated kinesin including 2 mg/mL of BSA, and 1 mM adenosine 5′-(β,γ-imino)triphosphate (AMP-PNP) solutions including MTs, followed by replacement with a motility assay buffer (1 mM adenosine triphosphate (ATP), 1.5% β-mercaptoethanol, 1.5 mg/mL BSA, 15 μM paclitaxel, 30 mM glucose, 120 μg/mL glucose oxidase, 30 μg/mL catalase, and 0.2% methylcellulose). The flow cell was incubated for 2 min between each step. To examine the methylcellulose dose-dependence of the event occurrence probabilities for gliding MTs over micro-grooves, high (0.5%) and low (0.1%) concentrations of methylcellulose solutions were also tested. The experiments were performed at a room temperature of 20 °C controlled by air conditioning. The sliding movements of the MTs were visualized using an inverted fluorescent microscope (IX-71, Olympus, Tokyo, Japan) equipped with a charge-coupled device (CCD) camera (Cascade 512B, Nippon Roper, Tokyo, Japan) and time-lapsed images of the gliding MTs were transferred to a personal computer (PC). Measurements of the MT extra lengths and incident angles of the MTs were conducted using image analysis software (ImageJ 1.42i, National Institutes of Health, Bethesda, MD, USA).

3. Results and discussion

Confirmation of bridging event of microtubules

Micro-scale grooves were fabricated on a Si substrate using microelectromechanical systems (MEMS) technology to form grooves with steep sidewalls with micrometer-scale control of the groove widths. Scanning electron microscope (SEM) images of the fabricated grooves are shown in Fig. 1B. The cross-sectional images show that the shape of the groove edges is a right angle. The widths of the grooves designed to be 2, 4, 6, and 10 μm were measured from the SEM images as 2.0, 4.0, 6.1, and 10.1 μm, respectively, which indicates that the groove widths were well

controlled. The depths of the grooves were also measured as 21, 23, 25, and 27 μm from SEM images for groove widths of 2, 4, 6, and 10 μm, respectively. In our preliminary experiments, the adhesion and motility properties of the gliding MTs on Si were not as good as those on glass coverslips, on which many previous studies have performed assays of gliding kinesin-driven MTs.[12] Therefore, the substrate was sequentially coated with Cr and Au layers, as previously reported.[13,14] As a result, the adhesion and motility properties on the Au substrate were confirmed to be comparable to those on glass coverslips (see ESI†).

A motility assay of the gliding MTs was then performed, according to a previously described technique.[9] A flow cell was fabricated with the prepared substrate and a coverslip, and kinesin motor proteins were then adsorbed onto the flow cell through a biotinylated BSA and streptavidin structure. By exchanging the solution in the flow cell with an assay solution including 1 mM ATP, the MTs began to glide in random directions along their long axis on the kinesin-coated surface. Some MTs approached the grooves on the surface (approaching area), seemed to bridge the grooves as previously reported[1] (Fig. 2, ESI movie 1†), and then continued their movement on the opposite surface of the groove (landing area). The fabricated grooves had depths of more than 20 μm, so that MTs gliding along the surface in the bottom of the grooves should have disappeared from the focal plane of the microscope. However, the MTs were observed to keep gliding over the grooves without disappearing from the focal plane. This confirmed the phenomena of groove bridging by the gliding MTs. It was found that the intensity of MTs within the grooves was less bright than that on the top surface of landing and approaching areas, even though its focal position was not changed. The phenomenon may be explained by the interference of fluorescence emitted from MTs and its reflection by the bottom of the grooves as reported by Kerssemakers *et al.*[15]

Relationship between length of bridging microtubules and groove width

To evaluate the relationships between the length of an MT (L_{MT}) and the width of a groove (W), length distributions of MTs approaching and bridging grooves were measured for 2, 4, 6, and 10 μm groove widths (Fig. 3). For all groove widths, many MTs that were longer than the groove widths exhibited bridging, whereas no bridging was observed for MTs shorter than the groove widths. This clearly indicates that bridging requires sufficient MT length so that the tips of the MTs can reach kinesins at the landing area. The result also implies that topographical grooves can be used to sort MTs longer than the groove width.

A motility property of kinesin-driven MTs was affected by kinesin densities as shown in our previous study.[9] In that study, MTs shorter than an estimated interval length between neighboring kinesins were likely to change the gliding direction, whereas MTs longer than the interval length were not. Since, for efficient transport systems, MTs are expected to glide in a straight trajectory, MTs longer than the interval length are preferred. On the other hand, very long MTs are not good carriers in terms of reducing the size of devices. Therefore, the present technique will be applicable to choose the suitable length of MTs.

Since taxol-stabilized MTs were used in this study, the changes in MT lengths for our observation were practically negligibly small (0.8 ± 0.5 μm for 10 min, $n = 10$). However, when a longer period of observation time than that in this study is required, MTs fixed with glutaraldehyde, which more stabilizes MT polymerization and depolymerization, would be a better option to keep their length constant. MTs pretreated with glutaraldehyde do not lose the activity of kinesin.[16]

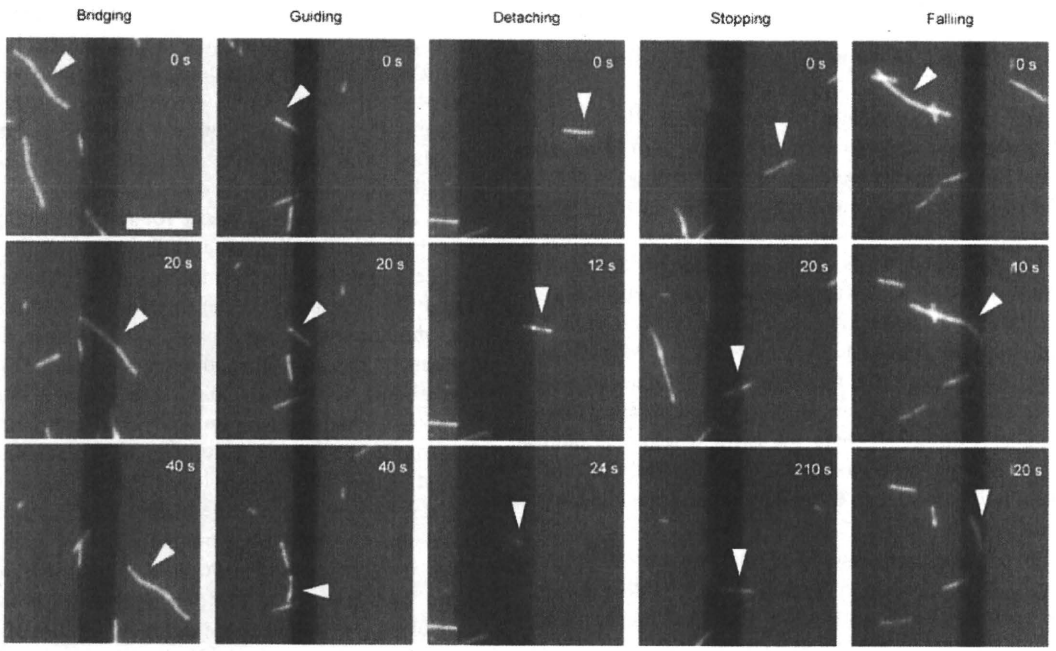

Fig. 2 Typical sequential images of gliding MTs approaching grooves. The MTs exhibited five unique events (white arrow heads): bridging, guiding, detaching, stopping, and falling. Scale bar = 10 μm. The groove widths are $W = 6$ μm (bridging), $W = 4$ μm (guiding), $W = 10$ μm (detaching), $W = 6$ μm (stopping), and $W = 4$ μm (falling).

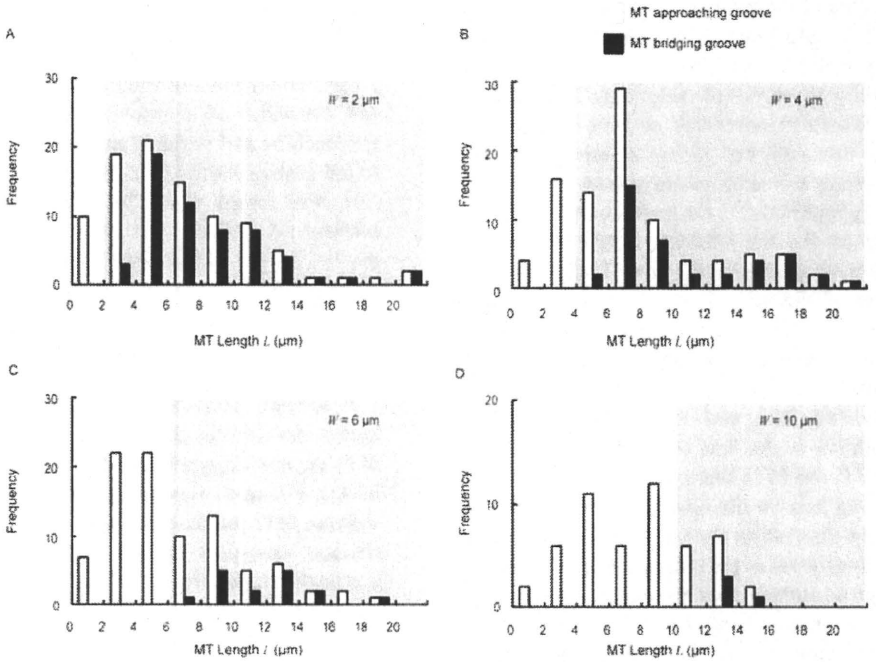

Fig. 3 MT length distributions for MTs approaching and bridging grooves. Only MTs longer than the groove width (shaded areas) exhibited bridging. The total numbers of MTs approaching the groove were (A) $n = 94$, (B) $n = 94$, (C) $n = 90$, and (D) $n = 52$.

Effect of topological conditions on event probabilities

In addition to bridging, MTs also exhibited the following unique behaviors: falling, guiding, detaching, and stopping (Fig. 2, ESI movie 2–5†). As reported previously,[1] some MTs fell into the grooves (falling). During guiding, the leading tips of the MTs overhung a groove from the approaching area and then reattached to kinesins on the approaching area. Detaching MTs detached from the surface over a groove. Stopping was defined as MTs that were immobile for more than 3 min at the edges of grooves.

To characterize the probability for each event, the effect of geometric parameters, such as the incident angle (α) and extra length of the MT compared to the groove width ($L_{MT} - W$), on the occurrence probability was analyzed. The incident angle represents the angle from the edge line of a groove, as shown in Fig. 4A. Fig. 4B shows plots of the extra length against the incident angle for each MT event. The bridging event occurred only for MTs with extra lengths larger than zero and at higher incident angles, and guiding tended to occur for MTs shorter than the groove width at lower incident angles. Plot distributions for stopping and detaching were similar and those events often occurred under conditions where the extra length was almost zero and the incident angle was high. The probability for all the events except falling seemed to depend on both the incident angle and the extra length.

According to these results, the MTs were categorized by their length, *i.e.*, $L_{MT} < W$, $L_{MT} > W$, and the probability was replotted for each event with respect to the incident angles (0–30°, 30–60°, and 60–90°) (Fig. 4C and 4D). In the case of $L_{MT} < W$, bridging did not occur as previously stated. The probability for guiding was 79% at $\alpha = 0$–30° and decreased with the increase in incident angle (55%, $\alpha = 30$–60°; 5%, $\alpha = 60$–90°). For larger incident angles, the probability for detaching and stopping increased. The falling event showed no dependency on either the incident angle or the extra length. In the case of $L_{MT} > W$, although the probability of bridging was low for lower incident angle (16% at $\alpha = 0$–30°), it tended to increase for larger incident angle (51% at $\alpha = 30$–60°) and reached 75% at $\alpha = 60$–90°. The guiding event was the most common event for smaller incident angle (53% at $\alpha = 0$–30°), and the occurrence probability decreased with increase of the incident angle (18%, $\alpha = 30$–60°; 3%, $\alpha = 60$–90°). The detaching and stopping events were rarely observed in the case of $L_{MT} > W$ (<10%), regardless of the incident angle. The probability for falling, in the case of $L_{MT} > W$, showed no dependency on either the incident angle or the extra length, as was the case for $L_{MT} < W$.

To develop a sorting device for MTs that utilizes MT events over grooves, the detaching, falling and stopping events would not be useful, because the motions of MTs showing these events cannot be controlled on the substrate. In contrast, the bridging and guiding events would be useful, because these MTs keep moving on the substrate and in the focal plane. Furthermore, the probabilities for bridging in the case of $L_{MT} > W$ and for guiding exhibited a dependence on the relationship between the MT length and the groove width, which indicates that MTs can be sorted by their difference in length. Therefore, we considered that a favorable condition for the sorting of MTs should satisfy all the requirements, *i.e.*, high probability for bridging in the case of $L_{MT} > W$, for guiding in the case of $L_{MT} < W$, and low probability for other events. The probabilities for both guiding in the case of $L_{MT} < W$ and for bridging in the case of $L_{MT} > W$ were higher at incident angles of 30–60°, as shown in Fig. 4C and 4D. From these results, it was supposed that control of the incident angle of gliding MTs to around 30–60° would result in a high

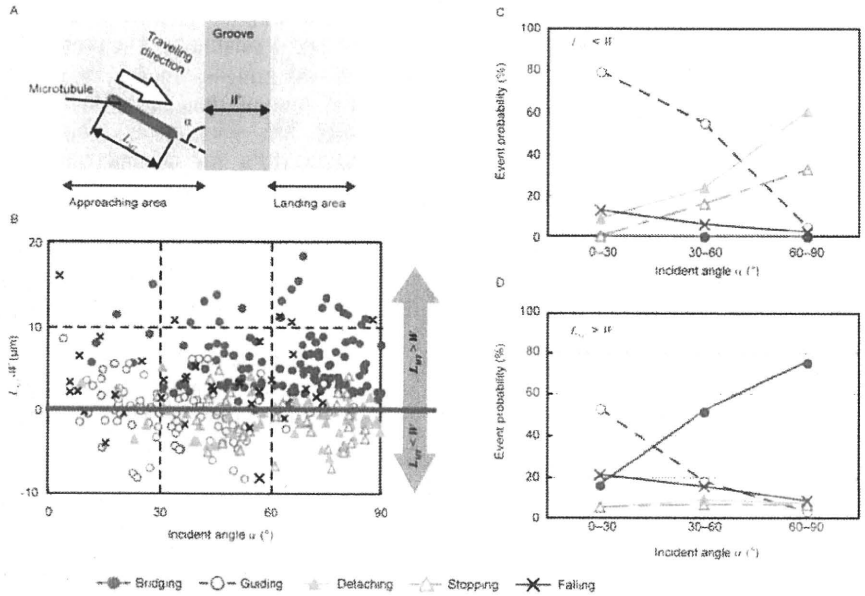

Fig. 4 Effect of the topological conditions of both grooves and MTs on the probability for each event. (A) Schematic illustration defining the parameters of MT length (L_{MT}), groove width (W), and incident angle (α) used for analysis. (B) Distribution of $L_{MT} - W$ against α for each event, which shows that all events except falling were likely to occur depending on both the $L_{MT} - W$ and the α parameters. (C and D) Probability for each event with respect to the incident angle α for (C) $L_{MT} < W$ and (D) $L_{MT} > W$.

probability for MT sorting according to their length. The incident angles of gliding MTs will need to be controlled in the future, *e.g.*, with a topological guide formed using a photoresist.[17] Furthermore, to prevent the MTs from crossing back from landing area to approaching area, rectifier structures should be equipped to those guides.[18] These systems enable separation the MTs by their length more effectively.

In the case of $L_{MT} < W$, the probabilities for detaching and guiding increased and decreased, respectively, as the incident angle increased. Clemmens *et al.*[19] reported that when the tips of MTs swept out from a kinesin-coated surface to a kinesin-free surface, they fluctuated and then reattached to the kinesin-coated surface with high probability in the case of smaller incident angle because the overhanging portion of the MT was easily bent back to the kinesin-coated surface at smaller incident angles. On the other hands, they also showed that many MTs detached from the kinesin-coated surface at larger incident angles. The experimental condition of no kinesin over the grooves used in this study was similar to that reported by Clemmens *et al.*, so that the detaching and guiding MTs observed in this study for smaller and larger incident angles, respectively, can be considered as basically the same events that they reported. In the case of $L_{MT} > W$, as the incident angle increased, the probability for bridging and guiding increased and decreased, respectively. The guiding of MTs should occur by the previously stated mechanism. For MTs approaching with smaller incident angles, the distances from the tips of the MTs to the kinesins on the approaching area are shorter than those on the landing area; therefore, they tend to reattach to the kinesins on the approaching area. On the other hand, for MTs approaching with the larger incident angles, it is easier to reattach to the kinesins on the landing area, resulting in a bridging event.

Ionov *et al.*[20] performed sorting of MTs using gradients of kinesin density on a surface. They changed kinesin density on a surface with polyethylene glycol (PEG) and showed that shorter MTs glided less with decreasing kinesin density, indicating the possibility of the size fractionation of gliding MTs. Like our study, their work also achieved the fractionation of MTs by their length without any additional devices. However, their technique, in principle, can not perfectly fractionate MTs by their length because it potentially includes longer MTs as well as shorter MTs on the surface with a high kinesin density. In contrast, in the present technique, MTs shorter than the groove width can be collected with the topographical guides as previously reported.[3] Furthermore, the present technique is more simple in fabrication compared to the one of Ionov *et al.*

The sorting technique in this study is applicable to other filament-type transporters such as the actin–myosin system, but there are some differences between MTs and actin filaments to be concerned with. One of the major differences is rigidity of filaments. Flexural rigidity of taxol-stabilized MTs was reported to be 2.2×10^{-23} N m^2, whereas that of actin filaments was 7.3×10^{-26} N m^2.[21] Since the flexural rigidity of actin filaments was lower than that of MTs, probabilities for events might be changed for actin transporters even in the same topographical conditions such as incident angle, groove width, and filament length. We thought that probability for guiding should be higher for an actin–myosin system than a kinesin-MT system, because softer actin filaments should easily be bent compared to MTs. Therefore, the optimum incident angle for sorting actin filaments by their length may be larger than that for MTs.

Effect of methylcellulose on event probability

The results suggest that the probabilities of the events are dependent on the thermal fluctuation of the MT tip. Therefore, the effects of various concentrations of methylcellulose, which is known to change the amplitude of thermal fluctuation,[22] on the probabilities of the events were investigated. Fig. 5 shows the probabilities of the events with respect to methylcellulose concentrations in the case of 30–60° incident angles, which is probably the suitable range of incident angle for MT sorting, based on the present results (Fig. 4). Although the stopping and falling events did not occur in the 0.1% methylcellulose solution, the probability for detaching was significantly increased for both $L_{MT} < W$ (83%) and $L_{MT} > W$ (48%) conditions. The probabilities for guiding with $L_{MT} < W$ and bridging for $L_{MT} > W$ increased as the methylcellulose concentration increased, and probabilities of approximately 70% were finally achieved in 0.5% methylcellulose solution (69% for guiding with $L_{MT} < W$, and 71% for bridging with $L_{MT} > W$). It should also be noted that the probability for detaching was low in the 0.5% methylcellulose solution. These results suggest that the probabilities of events can be regulated by changes in the concentration of the methylcellulose solution, which would result in the effective sorting of MTs.

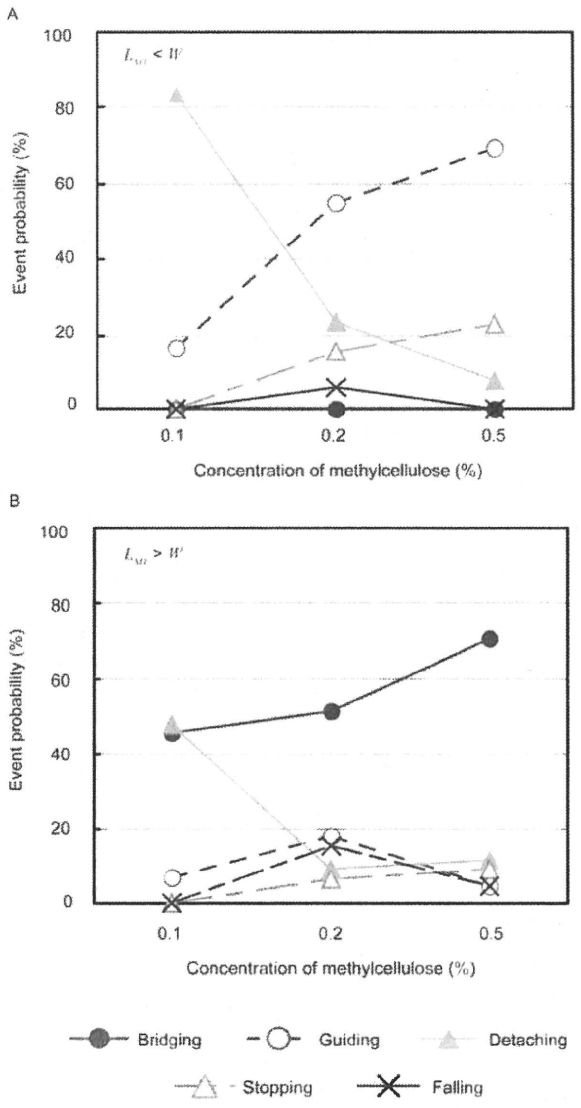

Fig. 5 Effect of methylcellulose concentration on the probability for each event. Event probabilities were calculated for (A) $L_{MT} < W$ and (B) $L_{MT} > W$ only in the case of incident angle $\alpha = 30$–$60°$, for which sorting of MTs by utilizing bridging and guiding events was considered to be effective.

The increase in the probability for bridging in a higher concentration of methylcellulose supports the hypothesis that the thermal fluctuation of MTs is a key factor for the probability of event occurrence. A higher concentration of methylcellulose suppresses Brownian motion, especially in the direction perpendicular to the MTs,[22] so that a decrease in the magnitude of MT bending results in an increase of attachments of the MT tips to the kinesins on the landing area. Thereby, the probability for bridging may be increased.

Detaching often occurred under conditions where the extra length ($L_{MT} - W$) was almost zero, indicating no contact between MTs and kinesins anymore. Our result also showed that the probability for detaching decreased in higher methylcellulose solutions. Since higher concentrations of methylcellulose have an effect to reduce fluctuations of filaments,[22] it is thought that MTs in higher methylcellulose solutions were kept near the surface and easily captured by kinesins. Taking together, it suggests that the decrease in interactions between kinesins and MTs caused the high probability for detaching.

It is unclear what physical conditions caused stopping and falling. The probability for stopping slightly increased with increasing methylcellulose concentration. We suppose that resistance to the driving force of kinesin acting MTs may increase under high methylcellulose condition. It was reported that an addition of methylcellulose caused an increase in viscosity of solutions[22] and high viscosity increased drag forces to MTs.[23] The increase in the stopping event may be explained by this finding. Falling seems to depend on neither the incident angle, the extra length, nor concentration of methylcellulose. Further investigations will be required for understanding the mechanisms of those events.

By regulating the methylcellulose concentration, the probabilities for bridging and guiding increased up to approximately 70%. This sorting efficiency is comparable to the result that van den Heuvel *et al.*[8] achieved under application of an electric field. Furthermore, the sorting of MTs was successfully achieved using only topographical grooves and without the need for any other devices such as for application of electric field or functions such as the detection of MTs. This technique enables the miniaturization of the sorting device; therefore, it has advantages for the development of nanoscale transport systems. Although many studies that have utilized topographical channels to control the sliding direction have been reported,[3,4] we have shown the feasibility of employing channels for the sorting of MTs. The principle of this sorting device will be a significant contribution to the development of nanoscale transport systems.

Conclusions

The behavior of kinesin-driven MTs over microscale grooves fabricated on a chip was characterized by five different events; bridging, guiding, detaching, stopping, and falling. The probabilities for these events were dependent on parameters such as the incident angle, the relationship between the MT length and groove width, and the concentration of methylcellulose solution. The probabilities for bridging and guiding attained approximately 70% in 0.5% methylcellulose for MTs shorter and longer than the groove width, respectively, which verified the feasibility of this technique for the development of a sorting device.

Acknowledgements

We thank Prof. Hideo Higuchi of the University of Tokyo for technical support and the preparation of proteins, and acknowledge the support of the Tohoku University Global COE Program, "Global Nano-Biomedical Engineering Education and Research Network Center".

References

1 H. Hess, C. M. Matzke, R. K. Doot, J. Clemmens, G. D. Bachand, B. C. Bunker and V. Vogel, *Nano Lett.*, 2003, **3**, 1651–1655.
2 M. G. van den Heuvel and C. Dekker, *Science*, 2007, **317**, 333–336.
3 H. Hess, J. Clemmens, D. Qin, J. Howard and V. Vogel, *Nano Lett.*, 2001, **1**, 235–239.
4 D. Riveline, A. Ott, F. Julicher, D. A. Winkelmann, O. Cardoso, J. J. Lacapère, S. Magnúsdóttir, J. L. Viovy, L. Gorre-Talini and J. Prost, *Eur. Biophys. J.*, 1998, **27**, 403–408.
5 M. Platt, G. Muthukrishnan, W. O. Hancock and M. E. Williams, *J. Am. Chem. Soc.*, 2005, **127**, 15686–15687.
6 R. Stracke, K. J. Böhm, J. Burgold, H.-J. Schacht and E. Unger, *Nanotechnology*, 2000, **11**, 52–56.
7 R. Stracke, K. J. Böhm, L. Wollweber, J. A. Tuszynski and E. Unger, *Biochem. Biophys. Res. Commun.*, 2002, **293**, 602–609.
8 M. G. van den Heuvel, M. P. de Graaff and C. Dekker, *Science*, 2006, **312**, 910–914.
9 S. Sugita, N. Sakamoto, T. Ohashi and M. Sato, *Journal of Biomechanical Science and Engineering*, 2008, **3**, 510–519.
10 Y. Inoue, Y. Y. Toyoshima, A. H. Iwane, S. Morimoto, H. Higuchi and T. Yanagida, *Proc. Natl. Acad. Sci. U. S. A.*, 1997, **94**, 7275–7280.
11 T. Kamei, S. Kakuta and H. Higuchi, *Biophys. J.*, 2005, **88**, 2068–2077.
12 J. Howard, A. J. Hudspeth and R. D. Vale, *Nature*, 1989, **342**, 154–158.
13 M. G. van den Heuvel, C. T. Butcher, S. G. Lemay, S. Diez and C. Dekker, *Nano Lett.*, 2005, **5**, 235–241.
14 M. G. van den Heuvel, C. T. Butcher, R. M. Smeets, S. Diez and C. Dekker, *Nano Lett.*, 2005, **5**, 1117–1122.
15 J. Kerssemakers, L. Ionov, U. Queitsch, S. Luna, H. Hess and S. Diez, *Small*, 2009, **5**, 1732–1737.
16 D. Turner, C. Chang, K. Fang, P. Cuomo and D. Murphy, *Anal. Biochem.*, 1996, **242**, 20–25.
17 S. G. Moorjani, L. Jia, T. N. Jackson and W. O. Hancock, *Nano Lett.*, 2003, **3**, 633–637.
18 Y. Hiratsuka, T. Tada, K. Oiwa, T. Kanayama and T. Q. Uyeda, *Biophys. J.*, 2001, **81**, 1555–1561.
19 J. Clemmens, H. Hess, R. Lipscomb, Y. Hanein, K. F. Bohringer, C. M. Matzke, G. D. Bachand, B. C. Bunker and V. Vogel, *Langmuir*, 2003, **19**, 10967–10974.
20 L. Ionov, M. Stamm and S. Diez, *Nano Lett.*, 2005, **5**, 1910–1914.
21 F. Gittes, B. Mickey, J. Nettleton and J. Howard, *J. Cell Biol.*, 1993, **120**, 923–934.
22 T. Q. Uyeda, S. J. Kron and J. A. Spudich, *J. Mol. Biol.*, 1990, **214**, 699–710.
23 A. J. Hunt, F. Gittes and J. Howard, *Biophys. J.*, 1994, **67**, 766–781.

Eur J Appl Physiol
DOI 10.1007/s00421-010-1779-x

SHORT COMMUNICATION

Skin advanced glycation end product accumulation and muscle strength among adult men

Haruki Momma · Kaijun Niu · Yoritoshi Kobayashi · Lei Guan · Mika Sato · Hui Guo · Masahiko Chujo · Atsushi Otomo · Cui Yufei · Hiroko Tadaura · Tatsunori Saito · Takefumi Mori · Toshio Miyata · Ryoichi Nagatomi

Accepted: 7 December 2010

Abstract Aging is associated with decreased skeletal muscle function. Increased levels of advanced glycation end products (AGEs) in skeletal muscle tissue are observed with advancing age and in diabetes. Although serum AGE level is negatively associated with grip strength in elderly people, it is unknown whether this association is present in adult males. To determine the relationship between AGE accumulation in tissue and muscle strength and power among Japanese adult men. Skin autofluorescence (AF) (a noninvasive method for measuring tissue AGEs), grip strength ($n = 232$), and leg extension power ($n = 138$) were measured in Japanese adult men [median (interquartile range) age, 46.0 (37.0, 56.0) years]. After adjustment for potential confounders, the adjusted means [95% confidence interval (CI)] for grip strength across the tertiles of skin AF were 44.5 (43.2, 45.9) kg for the lowest tertile, 42.0 (40.6, 43.3) kg for the middle tertile, and 41.7 (40.3, 43.1) kg for the highest tertile (P for trend < 0.01). Moreover, the adjusted geometric means (95% CI) of leg extension power across the tertiles of skin AF were 17.8 (16.6, 19.1) W/kg for the lowest tertile, 17.5 (16.4, 18.7) W/kg for the middle tertile, and 16.0 (14.9, 17.1) W/kg for the highest tertile (P for trend $= 0.04$). Among Japanese adult men, participants with higher skin AF had lower muscle strength and power, indicating a relationship between AGE accumulation and muscle strength and power. A long-term prospective study is required to clarify the causality.

Keywords Advanced glycation end products · Leg extension power · Grip strength · Carbonyl stress · Oxidative stress

Communicated by Arnold de Haan.

H. Momma · Y. Kobayashi · L. Guan · M. Sato · H. Guo · M. Chujo · A. Otomo · C. Yufei · H. Tadaura
Department of Medicine and Science in Sports and Exercise, Tohoku University Graduate School of Medicine, Sendai, Japan

K. Niu · T. Saito · R. Nagatomi (✉)
Division of Biomedical Engineering for Health and Welfare, Tohoku University Graduate School of Biomedical Engineering, 2-1 Seiryo-machi, Aoba-ku, Sendai 980-8575, Japan
e-mail: nagatomi@m.tains.tohoku.ac.jp

T. Mori · T. Miyata
United Centers for Advanced Research and Translational Medicine, Tohoku University Graduate School of Medicine, Sendai, Japan

Introduction

Ageing involves systemic accumulation of advanced glycation end products (AGEs), a diverse class of compounds resulting from glycation process under the strong influence of oxidative or carbonyl stress (Schleicher et al. 1997). In diabetic patients, increased accumulation of AGEs is observed (Schleicher et al. 1997; Singh et al. 2001). A common consequence of AGE accumulation is covalent cross-linking of AGEs to proteins, which leads to increased stiffness of protein matrix, impeding function and increasing resistance to removal of cross-linked proteins by proteolysis in various tissues and organs leading to impaired organ functions (Singh et al. 2001). Diabetic patients with end-stage renal disease had twice the concentrations of AGE in tissues compared with diabetic patients without renal disease (Makita et al. 1991).

Accumulation of AGE in the skeletal muscle tissue in elderly persons is suggested as one of the causes of decreased muscle force production (Haus et al. 2007).

Published online: 25 December 2010

Diabetic status accelerates AGE accumulation in skeletal muscle tissue in rats (Snow et al. 2006; Snow and Thompson 2009). In cross sectional studies, the levels of blood N^{ε}-carboxymethyl-lysine (CML), a major AGE in vivo, were negatively associated with muscle function in groups of elderly population (Dalal et al. 2009; Semba et al. 2010). Since AGE gradually accumulates along the course of aging even without diabetes, it is possible that the level of AGE accumulation may be inversely associated with muscle strength and power.

Using a simple autofluorescent measurement of AGE levels in the skin, we examined the association between AGE accumulation and muscle strength and power in a population of Japanese adult men.

Methods

Study participants

The study participants consisted of adult men, who had been enrolled in a prospective study of the risk factors for lifestyle-related illnesses or health status among adult employees in Japan. Participants received annual health examination including anthropometric measurements, hematological examinations and additional assessment including muscle strength and power measurement in year 2009. The details of this study have been described elsewhere (Guo et al. 2010).

The sample selection process is described in Fig. 1. In 2009, 1,263 participants were enrolled in the annual examinations for lifestyle-related illnesses and health status. Of those enrolled, 1,215 participants agreed to join the survey, providing their informed consent for data analysis (response rate, 96.2%). Because the number of female subjects was relatively small ($n = 282$), females were excluded from the analyses. Those who underwent skin AF measurement were randomly selected ($n = 518$). 272 participants who had lower skin reflection (<10%) were also excluded (details described in the skin autofluorescence section below). As a result of these exclusions, the numbers of subjects included in the analyses for the relationship between skin AF and grip strength (analysis I) and leg extension power (analysis II) were 232 and 138, respectively. The protocol of this study was approved by the Institutional Review Board of the Tohoku University Graduate School of Medicine.

Skin autofluorescence (AF)

Skin AGE accumulation was assessed based on skin AF using an autofluorescence reader (AGE Reader; Diagnoptics, Groningen, The Netherlands) as described previously

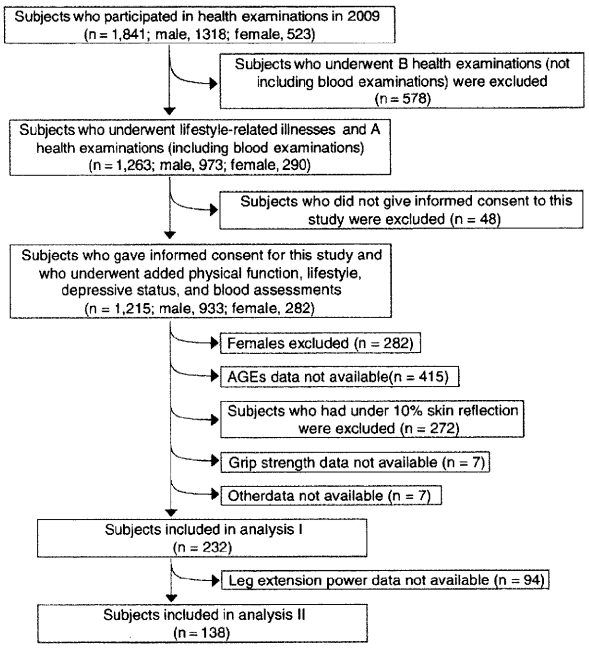

Fig. 1 Flow chart of the sample selection process

(Meerwaldt et al. 2004). The AGE Reader consists of a tabletop box equipped with an excitation light source. Each measurement took approximately 30 s to complete by an independent observer. Excitation light in the wavelength range of 300–420 nm is projected onto the skin surface through a 1-cm^2 hole. The intensity of light emitted from the skin at wavelengths between 420 and 600 nm is measured with a spectrometer via a glass fiber. Skin AF is calculated by dividing the mean value of the emitted light intensity per nm between 420 and 600 nm by the mean value of the excitation light intensity per nm between 300 and 420 nm; the result is expressed in arbitrary units (AU) and multiplied by 100 for easier evaluation. Skin AF has been validated to correspond to specific AGEs measured in human skin biopsy samples in several patient groups and healthy controls (Meerwaldt et al. 2004, 2005). The intra-assay coefficient of variation for repeated AF reader measurement on the same day was 5.0% (Meerwaldt et al. 2004).

All autofluorescence measurements were performed at room temperature on the volar side of the lower right arm, approximately 10–15 cm below the elbow fold, with the participants in a seated position. Care was taken to perform the measurement at a normal skin site, without visible vessels, scars, lichenification, or other skin abnormalities. The arm of each subject was covered with a black cloth in order to avoid any influence of external light during the measurement. Since skin pigmentation influences autofluorescence measurement, in particular when skin reflection is below 10%, autofluorescence values were not used